Abstract

Tactile shear force sensors are increasingly popular for medical applications especially for orthopedic rehabilitation such as measuring interfacial shear stresses between a residual limb and prosthetic socket to manage socket fit and residual limb tissue health, or measuring shearing between a foot sole and shoe for assessing performance in athletes. However, there are considerable challenges in implementing shear force sensors for orthopedic applications due to the requirements for noninvasiveness, light weight, low power, and robustness against motion artifacts, normal force, or electromagnetic fields. To address these challenges, this paper describes the design, fabrication, and characterization of a simple, low-cost, optoelectronic sensor that can measure multi-axial shear stresses. The sensor is based on a red, green, and blue (RGB) light-emitting diode (LED) cycling among red, green, and blue lights onto a color pattern surface. As shear strain causes a displacement between the LED and the color pattern, the relative intensities of reflected lights among the different colors change. A photodiode is used to capture the reflected light intensity at each color illumination, allowing the determination of the color pattern surface displacement, and in turn the shear, along two axes. In this paper, the efficacy of the sensor under benchtop testing conditions is reported, confirming the potential of this technology for shear monitoring at orthopedic devices such as protheses or shoes. Future efforts will focus on miniaturization and packaging of the sensors, and characterizing their performance for more medical and other types of applications.

Keywords: Shear force, strain, displacement, optical sensors, orthopedic rehabilitation, prosthesis.

1. Introduction

The utility of tactile shear sensors is rapidly increasing, particularly for robotics and medical applications [1], [2]. Within the field of robotics, shear sensors are useful for detecting slippage in grasping devices or ground contact dynamics in walking devices [1]. Among the many medical areas, the use of these sensors in orthopedic rehabilitation, such as measuring interfacial shear stresses between a residual limb and prosthetic socket, have been found to be impactful for managing socket fit and residual limb tissue health [3]–[5]. Furthermore, measuring shearing between a foot sole and shoe could lead to new innovations for assessing performance in athletes or managing tissue ulceration among individuals with diabetic neuropathy and/or dysvascular conditions. However, there are considerable challenges in implementing shear force sensors for orthopedic applications due to the specific requirements and constraints; shear sensors designed for the aforementioned uses should be mechanically imperceptible to the user and therefore must be packaged in a flexible housing and/or adopt a small footprint. In addition, the sensor must be light weight, have low power requirements, and be relatively unaffected by motion artifacts, normal force, or electromagnetic fields.

Many existing shear sensors are based on capacitive sensing principles [3]–[9], which often necessitate bulky packaging and are sensitive to electromagnetic interference from the environment, nearby mechatronic systems, or human body. For example, Sanders and Daly (1993) used metal-foil strain gauges embedded in the wall of a prosthetic socket to measure residual limb-prosthetic socket interfacial shear stresses. However, the bulk and mass of these sensors necessitated that holes be cut in the wall of socket, thus limiting their usefulness in clinical or daily use settings. Cheng et al. (2010) developed a polymer-based capacitive sensing array for normal and shear force measurement in robotics and orthopedics. This design is more flexible but has a larger footprint than the metal-foil strain gauges. It also offers a relatively limited shear sensing capacity (<1 N), making it impractical in for many robotic and orthopedic applications. Laszczak et al. (2015, 2016) developed a 3D-printed capacitive shear stress sensor. This sensor has a miniaturized design (20×20×4 mm), but is unable to differentiate between shear stresses along different axes.

In contrast to capacitive sensors, the optoelectronics counterparts are advantageous for measuring shear stress because they are generally thinner and are relatively unaffected by magnitude of normal force [10]. Furthermore, devices based on optical sensing principles are unaffected by electromagnetic interference induced by the surroundings, human body, or other devices interacting with the sensor. A thin optical tactile shear sensor was developed and validated in [10]–[13]. This device senses shear stress based on optical coupling between a vertical-cavity surface-emitting later (VCSEL) and a photodiode, separated by a transparent elastomeric transducer layer. The sensor exhibited a repeatable sigmoidal relationship between photodiode current and shear stress for stresses up to 5 N. While this study made important progress toward the use of optical-based sensing techniques for measuring shear stress, the limited range of shear sensing, high power required to drive the VCSEL, and inability to measure directionality of shear stresses limit its utility for robotics and medical applications.

There remains a need for a miniaturized optical-based shear stress sensor with a scalable design that can be tuned to sense shearing of different magnitudes. The sensor should also be capable of differentiating directionality of the shear stresses and require low power. This paper describes the design and fabrication of a simple, low-cost, optoelectronic sensor for measuring multi-axial shear stresses. Sensor characterization and performance are reported. The present study investigated the efficacy of this sensor under benchtop testing conditions; future efforts will focus on miniaturization and packaging of the sensors, and characterizing their performance for more medical and other types of applications.

2. Methods

2.1. Operational Principles

The sensor measures multi-axial shear stresses based on optical coupling between red, green, and blue (RGB) light-emitting diode (LED) and a photodiode. This is a contactless design, meaning that all electronics and wiring are confined to one side of the sensor. A schematic of the sensing principles is shown in Figure 1. The instrumented side of the sensor has a windowed pattern (Figure 1, Surface A), whereas the opposite side of the sensor (Figure 1, Surface B) displays a colored grid consisting of green, red, blue, and magenta (red + blue) squares. The contactless design offers versatility in how the sensor is implemented. For example, the pattern on Surface B could be printed on a second sensor component as in Figure 1, or on an adjacent stationary surface or existing device (e.g., a shearing body on a robot). Controlling electronics cycle the LED color while measuring reflected light intensity as a resistance change at the photodiode during red (R_r), green (R_g), and blue (R_b) light illumination.

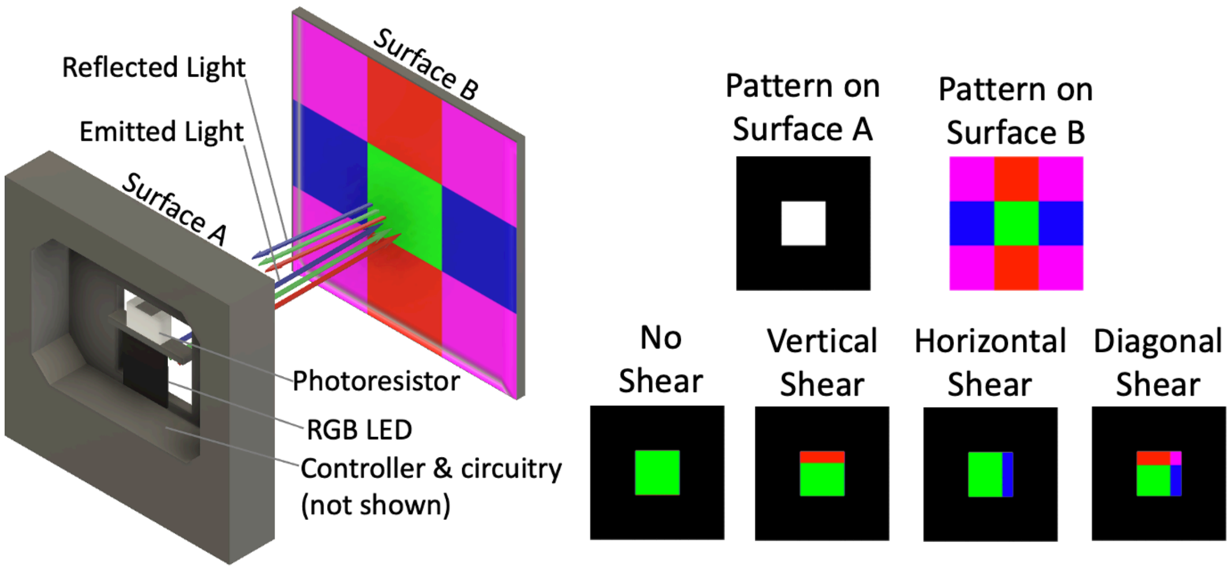

Figure 1. (Left) Illustration of the operational principle of the contactless optoelectronic shear sensor. (Right) Schematic diagram of shear sensing principles based on optical coupling between the RGB LED and photoresistor.

When there is no shear force applied to the sensor, Surfaces A and B are perfectly aligned, and thus only green appears in the window on Surface A (Figure 1, right). Under this condition, the photodiode only measures a resistance change when the LED is emitting green light, since there is no blue or red color surface to reflect the blue and red light, respectively ($R_g > 0$, $R_r = R_b = 0$). A vertical shear force causes misalignment of Surfaces A and B, and the red squares on Surface B are exposed through the window of Surface A, leading to resistance changes in R_g and R_r. The values for R_g and R_r are inversely proportional and proportional to the magnitude of vertical shear force, respectively. Similarly, a horizontal shear force causes the blue on Surface B to be visible in the window on Surface A. When the sensor experiences both vertical and horizontal shear forces, the magenta surface appears through the opening of Surface A, which reflects both blue and red lights. As a result, vertical shear force can be calculated as the ratio R_r / R_g, and horizontal shear force can be determined as R_b / R_g.

2.2. Sensor Architecture and Fabrication

The sensor is comprised of three main components: an instrumented housing for the LED, photodiode, and circuitry; a color pattern (Surface B) and a black window (Surface A); and an intermediate optically clear deformable layer made of polydimethylsiloxane (PDMS) elastomer layer (Sylcap, MicroLubrol, Clifton, NJ) separating Surfaces A and B (Figure 2). The sensor packaging, including circuitry, is 15 mm × 15 mm × 5 mm. To maintain accuracy, the thickness of the sensor is largely dependent upon the thickness of the deformable layer: the thicker the layer, the larger the size for Surface A and B. The range of shear stress magnitudes and sensitivity to changes in shear stress can be tuned by changing the PDMS thickness and curing conditions, which affects the stress-strain property of the material [14].

The LED (DotStar APA102-2020, Shenzhen LED Color Opto Electronic Co., Shenzhen, China) is 2 mm × 2 mm × 0.9 mm and emits red, green, and blue light at 620 nm, 520 nm, and 465 nm wavelengths, respectively. At 20 mA, the brightness for these colors is 300-330 mcd (millicandela), 420-460 mcd, and 160-180 mcd. The photodiode (Vishay Semiconductors, VEMD1060X01, Shelton, CT) is 1 mm × 2 mm × 0.9 mm with a 0.2 mm^2 active area. The photodiode is sensitive to wavelengths ranging from 350 nm to 1070 nm, which is inclusive of the red, green, and blue color spectra. The LED and photodiode are mounted to a printable circuit board (PCB) (OshPark, Lake Oswego, OR) which is housed in a 3D printed methylacrylate photopolymer resin (Figure 2). By employing rapid prototyping technology in the fabrication process, the sensor's cost-efficiency and versatility are improved. Within the housing, the LED and photoresistor are isolated such that photoresistor is only exposed to light reflected from Surface B.

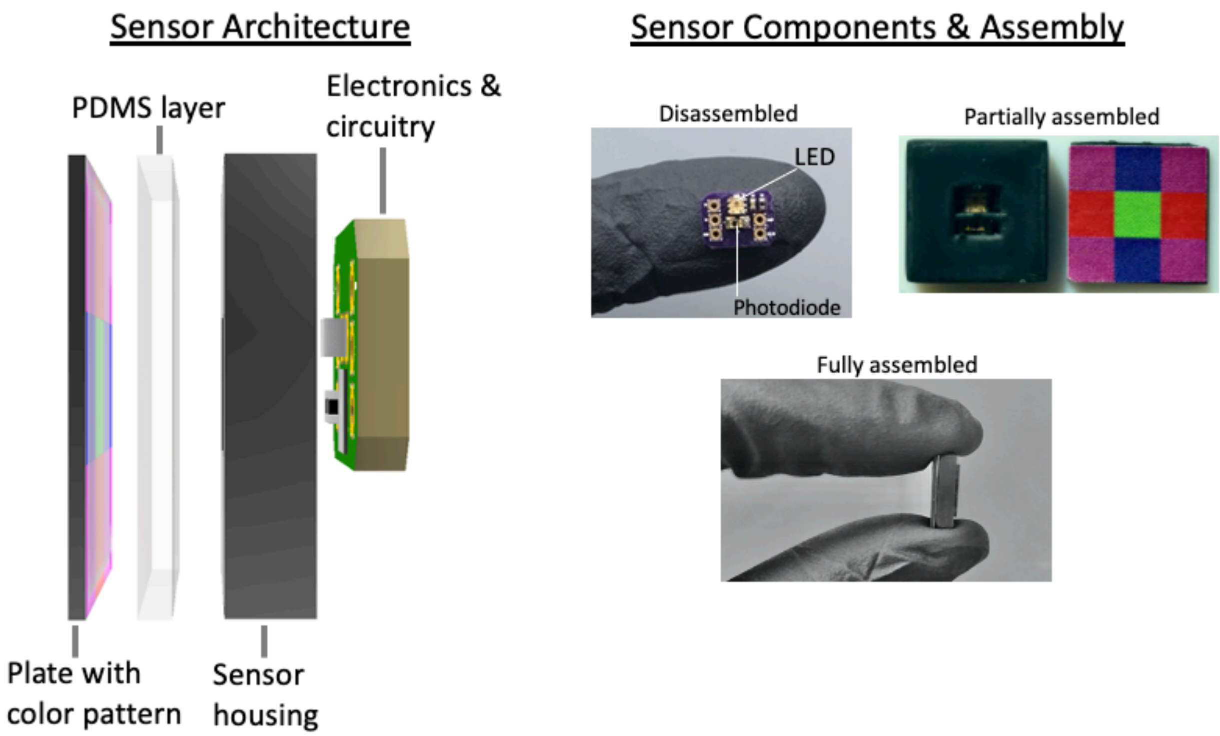

A B

Figure 2. (A) 3D illustration of the sensor components. **(B)** Partially populated circuit board for the sensor featuring the LED and photodiode (left); partially assembled sensor without elastomer layer (right); and fully-assembled sensor and circuitry (bottom).

A resin mold for the PDMS elastomer layer (Sylcap, Microlubrol, Clifton, NJ) was 3D printed and adhered to a Teflon plate. The base agent and curing agent were poured into the mold and cured at room temperature for 24 hrs. After curing, the PDMS elastomer was removed from the mold trimmed to the dimensions of the sensor housing, and adhered to Surfaces A and B of the sensor (Loctite 401, Düsselforf, Germany). In a previous material characterization studies, the shear modulus of PDMS at room temperature was found to be 250 - 450 kPa [10], [15]. However, the material properties of PDMS are known to be tunable by adjusting the geometry and curing parameters of the elastomer [14]. The mass of the sensor is 1.01 g.

2.3. Sensor characterization

The sensor response to both displacement and applied shear force were measured. Measuring the response to displacement serves to establish the sensitivity of the sensor towards change in strain. Measuring the response to shear stress is useful to further characterize the sensor's performance under the ultimate use case conditions.

To apply controlled displacement, a 3D-printed housing was designed to secure the sensor components in a materials testing system (EnduraTEC ELF, TA Instruments, New Castle, DE) (Figure 3). For displacement tests, a 3 mm-thick spacer was placed between the two sides of sensor in place of the elastomer. The instrumented side of the sensor (Surface A) was displaced with respect to the Surface B in 1 mm increments up to 10 mm. At each 1 mm position, a static measurement of RGB color intensity was recorded by cycling each LED color 10 times at 50 Hz and recording the average of the 10 measurements for each color. To measure the repeatability of the sensor, 5 trials were completed, and inter-trial variability was calculated. These measurements were then repeated in the horizontal direction. Sensor-derived measurements of displacement were then compared to measurements from the materials testing system's integrated High Accuracy Displacement Sensor (HADS) (EnduraTEC ELF, TA Instruments, New Castle, DE).

To characterize the sensor's performance for measuring shear stress, a 3 mm-thick optically-clear PDMS elastomer layer was adhered between Surfaces A and B. The sensor was then placed in the materials testing system using the methods described above. The materials testing system was actuated for loads ranging 0 – 20 N in 2.5 N increments, measured via a load cell (1516FQG-100, TA Instruments, New Castle, DE) placed in series with the actuator. Red, green, and blue color intensity was measured as a resistance at the photodiode during each static load increment. Each LED color was cycled 10 times at 50 Hz and the average resistance was recorded for each color. To measure the repeatability of the sensor, 5 trials were completed and inter-trial variability was calculated. Sensor-derived measurements of shear stress were then compared to data from the load cell. Hysteresis of the sensor was also characterized. All data were collected in dark conditions to avoid interference from ambient light sources.

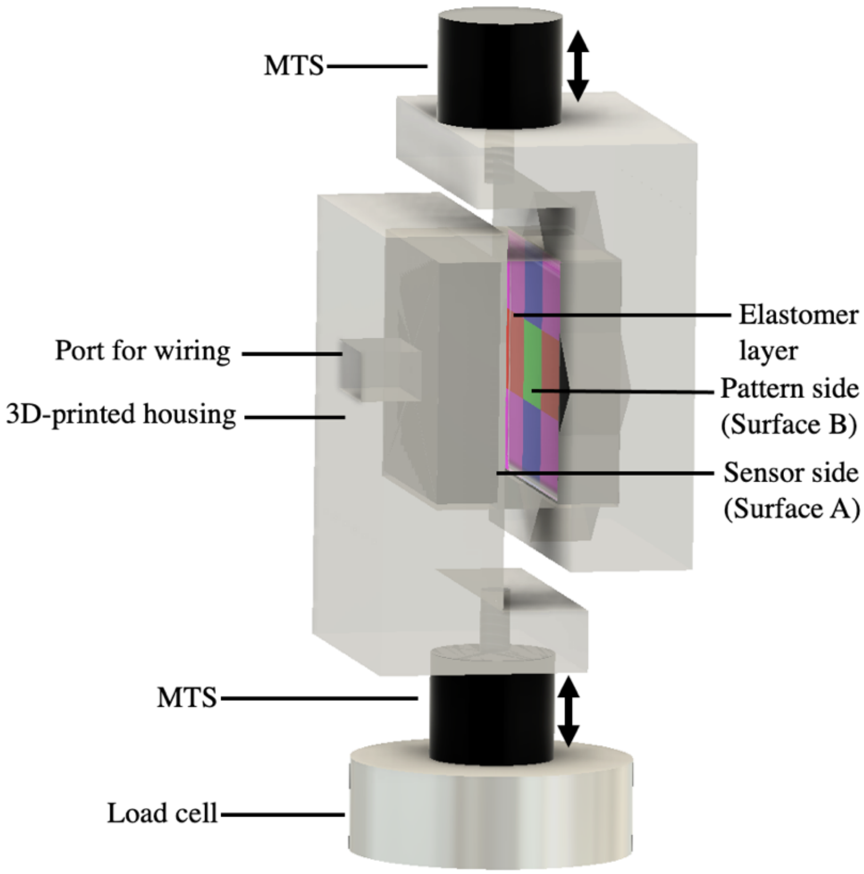

Figure 3: Rendering of setup for translational testing of the sensor. The MTS actuates vertically, displacing the instrumented side of the sensor (Surface A) with respect to Surface B. Displacement and force are measured via an integrated displacement sensor and load cell, respectively. Surface B can be rotated within the housing to displace horizontally or vertically.

2.4. Data analysis

Displacement data measured from the HADS (accuracy: ± 0.0001 mm) and load data from the in-series load cell (accuracy: ± 0.0001 N) were used as gold-standard comparator values to model and characterize the sensor's performance. The ratio R_r / R_g was used to for quantifying displacement/shear stress changes in the vertical direction, whereas R_b / R_g was used for quantifying horizonal changes. For both displacement and shear stress, a model fit was derived for the sensor's response (i.e., light intensity) compared to the gold standard value.

Gaussian Process (GP) regression was used to model the sensor response for both the displacement and shear stress conditions (Mathworks, Natick, MA). Compared to traditional regression models, GPs are advantageous for characterizing sensor performance because they can directly capture model uncertainty in addition to predicted values. Further, the user may add *a priori* knowledge and specifications about the shape and behavior of the model by selecting different kernel functions (e.g., linear vs exponential). Five rounds of cross-validation were performed using randomized data partitions. The validation results were averaged across the rounds to give an overall characterization of the model's predictive performance. Sensor performance was characterized using coefficient of determination (R^2), mean absolute error (MAE), and root-mean-squared error (RMSE) values across the full range of conditions tested.

3. Results and Discussion

3.1. Sensor Performance

Sensor-derived measurements of horizontal displacement matched HADS values well ($R^2 > 0.99$, MAE = 0.08 mm, RMSE = 0.20 mm) (Figure 4). The sensor showed similar performance for vertical displacement ($R^2 > 0.99$, MAE = 0.07 mm, RMSE = 0.16 mm) (Figure 4). These data serve to demonstrate the baseline performance of the sensor's operating principle of measuring optical coupling between the RGB LED and photodiode, essentially based on the light reflected from the patterned color surface. Inter-trial variability was < 0.02%, indicating that the sensor is capable of making repeatable measurements. Higher residuals (~1 mm) for displacements of 1 mm in both the horizontal and vertical directions indicate that the sensor may not be sensitive to displacements < 1 mm. This parameter may be tunable through sensor design modifications such as LED light intensity or use of an amplifier.

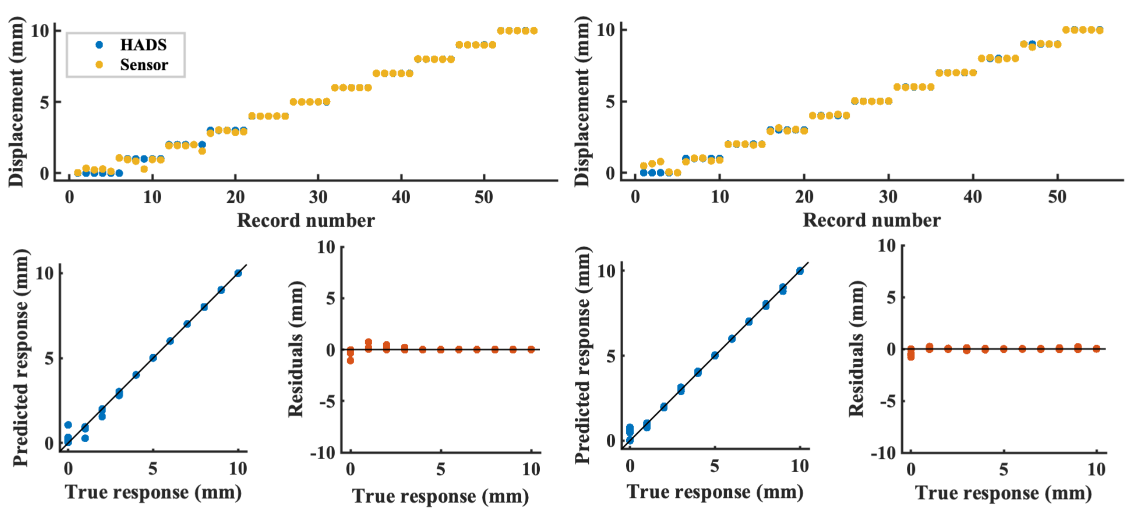

A B

Figure 4: Performance of sensor compared to High Accuracy Displacement Sensor (HADS) for measuring horizonal (left) and vertical (right) displacements.

The sensor's performance for measuring shear stresses in the horizontal and vertical directions showed greater variability compared to displacement measurements. Nevertheless, sensor-derived measures of horizonal shear stress matched load cell data well ($R^2 > 0.96$, MAE = 0.97 N, RMSE = 1.2 N) (Figure 5). Performance in the vertical directional was more accurate and exhibited decreased variability compared to the horizonal direction ($R^2 > 0.98$, MAE = 0.91 N, RMSE = 0.9 N) (Figure 5). The decreased accuracy for shear measurements compared to displacement could be due to the fact that sensor fabrication is still in a preliminary prototyping stage. It is possible that the deformation of the PDMS layer is not completely homogenous, resulting in decreased accuracy for sensor-derived measurements of shear stress. It is also possible that the methods used to adhere the PDMS to Surfaces A and B was insufficient and some slippage occurred.

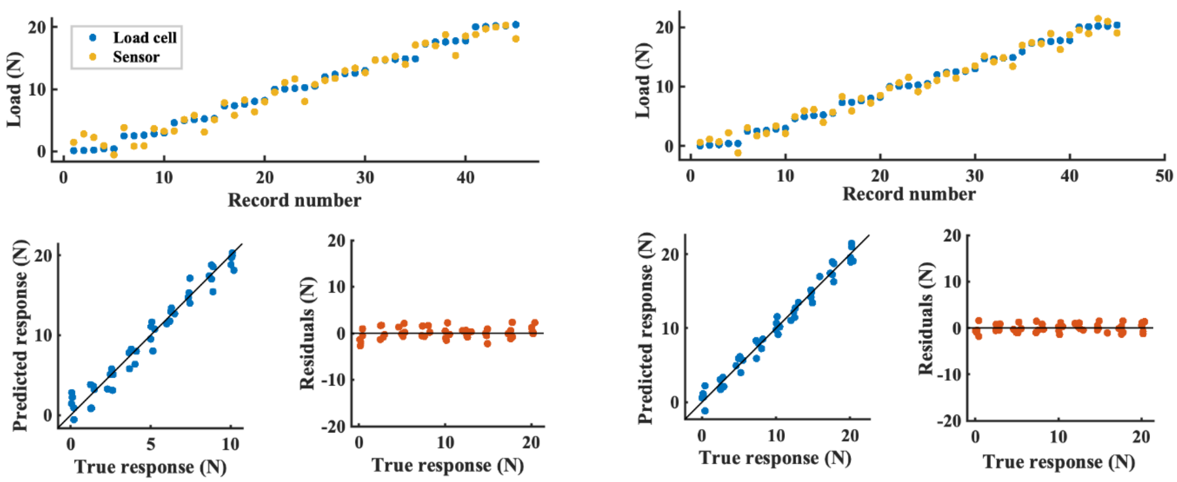

A B

Figure 5: Performance of sensor compared to the load cell for measuring (A) horizonal and (B) vertical shear stresses.

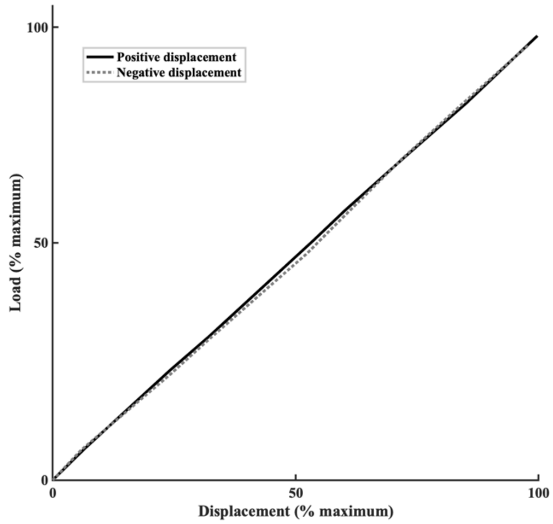

Figure 6: Hysteresis response for sensor measured via HADS and load cell.

To investigate the elastic behavior of the physical sensor package (i.e., PDMS elastomer, assuming the resin housing is rigid) the stiffness and hysteresis were evaluated. The sensor exhibited a linear relationship between load and displacement ($R^2 > 0.99$) as measured via the load cell and HADS. Hysteresis was < 0.1% across the full range of loads and displacements (Figure 6). The relationship between force (F) and displacement (x) was 13.4 N/mm and the PDMS layer has a surface area (A) of 50 mm^2. As such, the shear modulus (G) of the sensor's PDMS can be calculated as function of force, displacement, and PDMS area (Eq. (1)), assuming complete rigidity of the resin housing.

$$\mathrm{G} = \frac{F/x}{A} = \frac{13.4\ N/mm}{45\ mm^2} = 298\ kPa \qquad \text{Eq. (1)}$$

The calculated modulus of 298 kPa is similar to the values reported in previous characterizations of the material properties of PDMS [14], [15]. The modulus of PDMS can also be tuned based on different curing parameters [10], [14], [15], which makes this design scalable to meet different loading requirements. Values between 0.93 mPa and 450 kPa have been reported [10], [14].

The goal of this work was to develop a simple and low-cost shear stress sensor that meets a variety of constraints associated with use in robotics, as well as medical applications especially orthopedic rehabilitation. The linearity, scalability, and resolution in shear stress measurements derived from this sensor support its use for these applications. High linearity is advantageous, as it can potentially allow for simplified sensor calibration and minimal signal conditioning requirements for signal processing. The scalability is also beneficial to the adoption by other applications, as many previous shear sensor designs were limited in their uses due to low sensing range [6], [9], [10]. High sensor resolution is important for a variety of uses. For example, sensor feedback could be used to allow a grasping robot to handle a fragile object by providing the necessary grip force to manipulate the object without breaking it. In medicine, pressure of <8 kPa can cause tissue ischemia [16], thus necessitating high resolution for sensors tasked with identifying these conditions. Shear stress has been shown to be at least equivalent to pressure as an external factor leading to tissue breakdown [17], and thus, high resolution for shear measurements from this sensor show promise for providing early indication of tissue breakdown.

Data show differentiation between horizonal and vertical shear stresses and indicate that the sensor performs equally well in both dimensions. This quality of this technology is especially high compared to previous work in optical-based shear sensors which were only capable of sensing resultant shear stress [10]–[13]. The ability to measure multi-axial shear stresses has typically been limited to strain gauges [4], [18], [19]. However, compared to this sensor, strain gauges are often larger (e.g., 47 mm [4]), heavier (e.g., 375 g [18]), require greater power, and necessitate being tethered by cables [20]–[25]. The technology shown in this paper exhibit both desirable sensing performance of the strain gauges and physical/electrical characteristics of other optical sensors.

3.2. Current Limitations and Future Directions

Future work should seek to characterize the long-term performance of the sensor. It remains unclear if periodic recalibration will be necessary to account for deterioration of the elastomer layer. Similarly, the sensor's performance should be characterized under a variety of environmental conditions (e.g., temperature) as the material properties of elastomers are known to fluctuate based on varied conditions [26].

A robust characterization of the sensor's response to multi-axial shear stresses will be necessary for many applications. The present experimental setup only allowed for evaluation of the sensor along the horizonal and vertical axes. While data indicate that the sensor is capable of differentiating between vertical and horizonal shear stresses, its capacity to correctly identify off-axis (i.e., a combination of vertical and horizonal) shearing remains unknown. Future work should test this ability. Similarly, future work should evaluate the dynamic scalability of the sensor by testing various loading rates.

Reducing the size of the sensor is an important next step to maximize its utility by reducing invasiveness. This could be achieved by sourcing smaller integrated components or using different materials for housing, such that size can be minimized without sacrificing strength. Modifying the present sensor design to meet the requirements of different applications is also an important next step. For example, some applications may benefit from a flexible design, which could be achieved through use of flexible printable circuit boards. Currently, the use of rapid fabrication techniques (e.g., 3D printing and use of PCBs) in the construction of this sensor are advantageous for quickly designing, implementing, and testing modifications. However, future manufacturing process may rely on traditional mass fabrication methods such as injection molding and automated circuit population to improve sensor-to-sensor repeatability and manufacturing speed.

4. Conclusions

This work presented a novel method for sensing shear stress based on coupling between light from and LED reflected off a patterned color grid and a photodiode. A sensor based on these principles was fabricated and characterized. The sensor demonstrated robust and accurate measurements of multi-axial displacements and shear stresses. These properties, along with its small, low-cost, and scalable design support the use of this sensor for a variety of applications in robotics, medicine, and orthopedics.

Funding sources:

This project is partially supported by the University of Oregon Venture Launch’s Translation Research Grant and University of Oregon’s Knight Campus Start Up fund.

[1] A. M. M. Yardley and K. D. Baker, "Tactile Sensors for Robots: A Review," in *The World Yearbook of Robotics Research and Development*, Springer Netherlands, 1986, pp. 47–83.

[2] M. I. Tiwana, S. J. Redmond, and N. H. Lovell, "A review of tactile sensing technologies with applications in biomedical engineering," *Sensors and Actuators, A: Physical*, vol. 179. Elsevier B.V., pp. 17–31, 01-Jun-2012.

[3] P. Laszczak *et al.*, "A pressure and shear sensor system for stress measurement at lower limb residuum/socket interface," *Med. Eng. Phys.*, vol. 38, no. 7, pp. 695–700, Jul. 2016.

[4] J. E. Sanders and C. H. Daly, "Measurement of Stresses in Three Orthogonal Directions at the Residual Limb-Prosthetic Socket Interface," *IEEE Trans. Rehabil. Eng.*, vol. 1, no. 2, pp. 79–85, 1993.

[5] P. Laszczak, L. Jiang, D. L. Bader, D. Moser, and S. Zahedi, "Development and validation of a 3D-printed interfacial stress sensor for prosthetic applications," *Med. Eng. Phys.*, vol. 37, no. 1, pp. 132–137, Jan. 2015.

[6] M.-Y. Cheng, C.-L. Lin, Y.-T. Lai, and Y.-J. Yang, "A Polymer-Based Capacitive Sensing Array for Normal and Shear Force Measurement," *Sensors*, vol. 10, pp. 10211–10225, 2010.

[7] R. A. Brookhuis *et al.*, "Six-axis force–torque sensor with a large range for biomechanical applications," *J. Micromechanics Microengineering*, vol. 24, no. 3, p. 035015, Mar. 2014.

[8] J. E. Sanders, C. H. Daly, and E. M. Burgess, "Interface shear stresses during ambulation with a below-knee prosthetic limb," *J. Rehabil. Res. Dev.*, vol. 29, no. 4, pp. 1–8, 1992.

[9] E. Choi *et al.*, "Highly sensitive tactile shear sensor using spatially digitized contact electrodes," *Sensors (Switzerland)*, vol. 19, no. 6, Mar. 2019.

[10] J. Missinne *et al.*, "Ultra thin optical tactile shear sensor," *Procedia Engineering*, vol. 25. Elsevier, pp. 1393–1396, 01-Jan-2011.

[11] J. Missinne *et al.*, "Flexible shear sensor based on embedded optoelectronic components," *IEEE Photonics Technol. Lett.*, vol. 23, no. 12, pp. 771–773, 2011.

[12] J. Missinne, E. Bosman, B. Van Hoe, G. Van Steenberge, P. Van Daele, and J. Vanfleteren, "Embedded flexible optical shear sensor," *Proc. IEEE Sensors*, pp. 987–990, 2010.

[13] J. Missinne *et al.*, "Two axis optoelectronic tactile shear stress sensor," *Sensors Actuators,*

A Phys., vol. 186, pp. 63–68, 2012.

[14] L. C. S. Nunes, "Shear modulus estimation of the polymer polydimethylsiloxane (PDMS) using digital image correlation," *Mater. Des.*, vol. 31, no. 1, pp. 583–588, Jan. 2010.

[15] J. C. Lötters, W. Olthuis, P. H. Veltink, and P. Bergveld, "The mechanical properties of the rubber elastic polymer polydimethylsiloxane for sensor applications," *J. Micromechanics Microengineering*, vol. 7, no. 3, pp. 145–147, 1997.

[16] G. Allen Holloway, C. H. Daly, D. Kennedy, J. Chimoskey, C. H. Dalyjion Kennedy, and J. Cwr, "Effects of external pressure loading on human skin blood flow measured by 133Xe clearance," 1976.

[17] M. Zhang, A. R. Turner-Smith, V. C. Roberts, and A. Tanner, "Frictional action at lower limb/prosthetic socket interface," in *Medical Engineering and Physics*, 1996, vol. 18, no. 3, pp. 207–214.

[18] J. E. Sanders, C. H. Daly, and E. M. Burgess, "Interface shear stresses during ambulation with a below-knee prosthetic limb," *J. Rehabil. Res. Dev.*, vol. 29, no. 4, pp. 1–8, 1992.

[19] J. E. Sanders, A. Karchin, J. R. Fergason, and E. A. Sorenson, "A noncontact sensor for measurement of distal residual-limb position during walking," *J. Rehabil. Res. Dev.*, vol. 43, no. 4, pp. 509–516, 2006.

[20] A. Courtney, M. S. Orendurff, and A. Buis, "Effect of alignment perturbations in a trans-tibial prosthesis user: A pilot study," *J. Rehabil. Med.*, vol. 48, no. 4, pp. 396–401, 2016.

[21] M. R. Safari, N. Tafti, and G. Aminian, "Socket Interface Pressure and Amputee Reported Outcomes for Comfortable and Uncomfortable Conditions of Patellar Tendon Bearing Socket: A Pilot Study," *Assist. Technol.*, vol. 27, no. 1, pp. 24–31, Jan. 2015.

[22] A. Schiff *et al.*, "Quantification of Shear Stresses Within a Transtibial Prosthetic Socket.," *Foot ankle Int.*, vol. 35, no. 8, pp. 779–782, Aug. 2014.

[23] H. Gholizadeh, N. Azuan, A. Osman, A. Eshraghi, N. Anuar, and A. Razak, "Clinical implication of interface pressure for a new prosthetic suspension system," *Biomed. Eng. Online*, vol. 13, no. 89, 2014.

[24] S. Ali, N. A. Abu Osman, A. Eshraghi, H. Gholizadeh, N. A. Bin Abd Razak, and W. A. B. Bin Wan Abas, "Interface pressure in transtibial socket during ascent and descent on stairs and its effect on patient satisfaction," *Clin. Biomech.*, vol. 28, no. 9–10, pp. 994–999, Nov. 2013.

[25] E. Boutwell, R. Stine, A. Hansen, K. Tucker, and S. Gard, "Effect of prosthetic gel liner thickness on gait biomechanics and pressure distribution within the transtibial socket," *J. Rehabil. Res. Dev.*, vol. 49, no. 2, pp. 227–240, 2012.

[26] Y. Shi, M. Hu, Y. Xing, and Y. Li, "Temperature-dependent thermal and mechanical properties of flexible functional PDMS/paraffin composites," *Mater. Des.*, vol. 185, p. 108219, Jan. 2020.